Original Article

Inhibition of cGAS attenuates neonatal hypoxic-ischemic encephalopathy via regulating microglia polarization and pyroptosis

Haiyan Shen[1], Hongyi Lu[1], Liming Mao[2,3], Lei Song[1]^

[1]Department of Pediatrics, Nantong First People's Hospital (Affiliated Hospital 2 of Nantong University), Nantong, China; [2]Department of Immunology, School of Medicine, Nantong University, Nantong, China; [3]Basic Medical Research Center, School of Medicine, Nantong University, Nantong, China

Contributions: (I) Conception and design: L Song; (II) Administrative support: L Mao; (III) Provision of study materials or patients: H Lu; (IV) Collection and assembly of data: H Shen; (V) Data analysis and interpretation: H Shen; (VI) Manuscript writing: All authors; (VII) Final approval of manuscript: All authors.

Correspondence to: Lei Song, MD. Department of Pediatrics, Nantong First People's Hospital (Affiliated Hospital 2 of Nantong University), No. 666 Shengli Road, Chongchuan District, Nantong 226001, China. Email: ntyysl@163.com.

Background: Neonatal hypoxic-ischemic encephalopathy (HIE) is a condition causing brain injury in newborns with unclear pathogenesis. Cyclic GMP-AMP synthase (cGAS)/stimulator of interferon genes (STING) signaling pathway and NOD-like receptor protein 3 (NLRP3) mediated pyroptosis are thought to be involved in the pathological process of HIE, but whether these two mechanisms act independently is still unknown. Therefore, we aim to clarify whether there is any interaction between these two pathways and thus synergistically affects the progression of HIE.

Methods: The HIE model of neonatal rats was established using the Rice-Vannucci method. The potential therapeutic effect of RU.521 targeting cGAS on HIE was explored through rescue experiment. Twenty-four hours after modeling was selected as observation point, sham + vehicle group, HIE + vehicle group and HIE + RU.521 group were established. A complete medium of BV2 cells was adjusted to a glucose-free medium, and the oxygen-glucose deprivation model was established after continuous hypoxia for 4 hours and reoxygenation for 12 to 24 hours. 2,3,5-triphenyl tetrazolium chloride staining was employed to detect ischemic cerebral infarction in rat brain tissue, and hematoxylin and eosin staining was used to observe tissue injury. Immunofluorescence was applied to monitor the expression of cGAS. Real-time quantitative polymerase chain reaction and western blot were utilized to detect the expression of messenger RNA and protein.

Results: cGAS expression was increased in brain tissues of neonatal rats with HIE, and mainly localized in microglia. RU.521 administration reduced infarct size and pathological damage in rat HIE. Moreover, blocking cGAS with RU.521 significantly reduced inflammatory conditions in the brain by down-regulating STING expression, decreasing NLRP3 inflammasome activation and reducing microglial pyroptosis both *in vivo* and *in vitro*. Besides, RU.521 promoted the switching of BV2 cells towards the M2 phenotype.

Conclusions: This study revealed a link between the cGAS/STING pathway and the NLRP3/GSDMD/pyroptosis pathway in neonatal HIE. Furthermore, the small molecule compound RU.521 can negatively regulate cGAS/STING/NLRP3/pyroptosis axis and promote M2 polarization in microglia, which provides a potential therapeutic strategy for the treatment of neuroinflammation in HIE.

Keywords: Hypoxic-ischemic encephalopathy (HIE); cyclic GMP-AMP synthase inhibitor (cGAS inhibitor); NOD-like receptor protein 3 (NLRP3); pyroptosis; M1/M2 microglia

^ ORCID: 0000-0002-5388-9793.

Submitted Apr 18, 2024. Accepted for publication Aug 15, 2024. Published online Aug 28, 2024.
doi: 10.21037/tp-24-148
View this article at: https://dx.doi.org/10.21037/tp-24-148

Introduction

Neonatal hypoxic-ischemic encephalopathy (HIE) is a clinical syndrome characterized by neonatal brain injury due to fetal asphyxia during the perinatal period (1,2). The onset of this disease may also act as a trigger of many complications such as neonatal nervous system damage (3). Although the technologies in perinatal care have been largely improved in recent decades, some recent epidemiological investigations demonstrate that the incidence of neonatal HIE in both underdeveloped and developed countries is increasing (4), possibly due to the lack of a specific treatment for this disease. The reasonable diagnosis and treatment of neonatal HIE have always been the focus of medical attention. In addition to the conventional three-support and three-symptomatic measures, mild hypothermia is also a safe neuroprotective therapy for this disease and is now widely used in clinical practice. However, such measures are subject to multiple restrictions such as gestational age and time, and a small number of children will still be at risk of death after appropriate diagnosis and treatment (5,6). Therefore, clarifying the pathogenesis of neonatal HIE caused by asphyxia is of very important clinical value for the early prevention and treatment of neonatal HIE, as well as improving the prognosis of children.

Microglia is an important target cell in the early development of HIE (7,8). The increase of blood-brain barrier permeability and the release of inflammatory mediators modulated by microglia are important pathological mechanisms of HIE (9,10). Cyclic GMP-AMP synthase (cGAS)/stimulator of interferon genes (STING) signaling pathway widely exists in a variety of cells. It plays an important role in bacterial infection (11), viral infection (12), immune diseases (13), and inflammatory diseases (14). This pathway leads to the phosphorylation of nuclear factor kappa-B (NF-κB) inhibitor κB (IκB) and degradation through the ubiquitin-proteasome pathway. NF-κB enters the nucleus and induces an inflammatory cascade (15). The NOD-like receptor protein 3 (NLRP3) inflammasome is an innate immune-inflammatory protein complex that mediates the release of pro-inflammatory mediators, including IL-1β and IL-18 (16), thereby participating in the regulation of the inflammatory responses in many organs such as the heart, the kidney, the liver, and the lung (17-20). It has been reported that cGAS/STING and NLRP3-mediated pyroptosis are involved in the pathogenesis of HIE (21,22). However, the possible interaction between the cGAS/STING pathway and the NLRP3 inflammasome in HIE has not been clarified.

It is reported that after hypoxic-ischemic brain injury, activated microglia can be divided into classical activated M1 phenotype and selective activated M2 phenotype (23). The former is an activated ameboid-like shape and secrete excessive inflammatory factors and neurotoxic molecules, leading to the death of normal cells, while the latter is activated to secrete anti-inflammatory factors such as IL-10 and Arg-1, and has a stronger ability to engulf and clear apoptotic cells. The activation, polarization and mediated inflammatory response of microglia play an important role in the occurrence, development, and outcome of brain injury in HIE (24). A study has shown that RU.521 could promote microglial transformation from the M1 phenotype to the M2 phenotype and mitigate subarachnoid hemorrhage-induced brain injury (25). However, it is unknown how RU.521 affects microglia polarization in an HIE model.

Highlight box

Key findings

- RU.521 alleviated neuroinflammation in neonatal hypoxic-ischemic encephalopathy (HIE) by inhibiting the cyclic GMP-AMP synthase (cGAS)/stimulator of interferon genes (STING)/NOD-like receptor protein 3 (NLRP3)/pyroptosis axis and regulating M1/M2 balance.

What is known and what is new?

- Pyroptosis is involved in the pathophysiology of HIE, however, the particular molecular pathways of pyroptosis in HIE are unknown.
- This study revealed a link between the cGAS/STING pathway and the NLRP3/GSDMD/pyroptosis pathway in neonatal HIE, and it initially investigated the role of RU.521 in the modification of microglia polarization in HIE *in vitro*.

What is the implication, and what should change now?

- RU.521 played a beneficial role in HIE through the cGAS/STING/NLRP3 axis and improved HIE-induced pyroptosis in microglia.

In this study, we tried to answer if the cGAS/STING pathway has a synergistic effect with the NLRP3 inflammasome in the development of neonatal HIE. Using a microglial cell line and a rat model of HIE, we found that a cGAS inhibitor, RU.521, could significantly suppress the expression of cGAS and STING; meanwhile, it had an inhibitory role to NLPR3 mediated pyroptosis and the production of pro-inflammatory cytokines. More importantly, RU.521 significantly induced microglia M2 polarization. Our findings suggest that RU.521 could be a promising candidate for treating neonatal HIE via suppressing the cGAS/STING/NLRP3/pyroptosis axis and regulating microglia polarization. To our knowledge, this is the first study that links the cGAS/STING pathway and the NLRP3 inflammasome-mediated pyroptosis in an HIE model. We present this article in accordance with the ARRIVE reporting checklist (available at https://tp.amegroups.com/article/view/10.21037/tp-24-148/rc).

Methods

Animals

A total of 82 seven-day-old male and female Sprague-Dawley (SD) rats weighing 11–15 g were provided by the Center of Experimental Animals, Nantong University for the experiment, 10 pups died during the hypoxia procedure. These newborn animals were breast-fed and housed at 24±2 ℃ with a 12-hour light/dark cycle. All animal experiments were carried out under the approval of the Animal Ethics Committee of Nantong University, China (approval No. S20230610-099) and applied with the guide of the Animal Care and Use Committee of Nantong University.

Establishment of neonatal HIE model and drug administration

A protocol was prepared before the study without registration. Seven-day-old newborn SD rats were used to induce neonatal HIE model using the Rice-Vannucci method, a model that combined unilateral carotid artery ligation with an 8% oxygen concentration hypoxia model (26). In brief, SD rats were anesthetized with 3% isoflurane, and then fixed in the supine position, the left common carotid artery was identified, exposed, ligated, and cut. After surgery, the rats were returned to their mothers for 1 hour and then placed in a closed hypoxia box (8% oxygen, 92% nitrogen, flow rate 4 L/min) for 2.5 hours at 37 ℃. To investigate the effect of RU.521, pups were randomly divided into the sham group, HIE group and RU.521 group. In the sham operation group, only the carotid artery was exposed after anesthesia without ligation or hypoxia (26,27). RU.521 (5 mg/kg, HY-114180, MedchemExpress, Shanghai, China) was dissolved in 1% dimethyl sulfoxide (DMSO) + 10% corn oil + 7% N,N-dimethylformamide (DMF) + 82% saline at the concentration of 0.5 mg/mL and intraperitoneally injected at 2 and 12 hours post-HIE (28). The sham and HIE-only groups were intraperitoneally injected with an equal volume of solvent. All procedures were in compliance with EU Directive 2010/63/EU for animal experiments (29).

2,3,5-triphenyl tetrazolium chloride (TTC) staining

Twenty-four hours after the establishment of HIE, pups were sacrificed. The bilateral brain tissues of the rats were separated immediately and were taken in the coronal position. The tissues were divided into uniform 2 mm slices and incubated with 1% TTC solution for 20 minutes at 37 ℃ in the dark. The images were evaluated by Image-Pro plus software (red: normal brain area, white: infarct area). The percentage of infarct volume (%) = [contralateral volume (mm^3) – ipsilateral non-infarct volume (mm^3)]/[2× contralateral volume (mm^3)] ×100% infarcted volume (30). The experimenter was blind to the groups when reviewing and analyzing the stained slides.

Hematoxylin and eosin (H&E) staining

Brain, heart, liver and kidney tissues were fixed in 4% paraformaldehyde for 48 hours, then embedded in paraffin, cut into 4-μm slices, and stained with H&E. The photos were captured by a Nikon microscope (Nikon, Yokohama, Japan).

Immunohistofluorescence staining

Brain tissues were fixed in 4% paraformaldehyde for 48 hours and then dehydrated sequentially with 20% and 30% sucrose solutions. After being embedded in optimal cutting temperature compound (OCT), the tissues were cut into 12-μm slides. The brain sections were blocked with 5% sheep, 5% fetal serum, and 0.3% Triton X-100 for 2 hours at room temperature. Sections were incubated with the following primary antibodies at 4 ℃: mouse-anti-Iba1 (1:100, ab283319, Abcam, Waltham, MA, USA), mouse anti-glial fibrillary acidic protein (GFAP) (1:400, 3670, CST, Danvers, MA, USA), mouse-anti-NeuN (1:100, 94403,

CST) and rabbit-anti-cGAS (1:100, A8335, Abclonal, Woburn, MA, USA). After washing with phosphate buffered saline (PBS), the sections were incubated with fluorescent secondary antibodies in the dark for 2 hours at room temperature: goat anti-rabbit IgG H+L (Alexa Fluor™ 594) (1:1,000, A-21207, Invitrogen, Waltham, MA, USA) and goat anti-mouse IgG H+L (Alexa Fluor™ 488) (1:1,000, A-11001, Invitrogen). After washing with PBS, the sections were blocked in an antifade mounting medium with DAPI (P0131, Beyotime, Nantong, China). Finally, the photos were captured by a Nikon microscope.

TUNEL staining

Cell apoptosis was detected using the terminal deoxynucleotidyl transferase deoxyuridine nick-end labeling (TUNEL) kit (C1090, Beyotime). In summary, brain tissue sections fixed in paraffin were dewaxed and then treated for 30 minutes at room temperature with proteinase K (20 μg/mL, ST533, Beyotime). After washing with PBS, the sections were incubated at 37 ℃ in the dark for 60 minutes for incubation with the TUNEL reaction mixture. Finally, after the sections were washed in PBS, the nuclei were counterstained with DAPI (BMU107, Abbkine, Wuhan, China). The photos were captured by a Nikon microscope. TUNEL-positive cells were quantified as a percentage of the total number of nuclei.

Renal and hepatic function evaluation

Blood samples were collected at 24 hours after the establishment of HIE and centrifuged at 2,500 rpm for 10 minutes. The upper serum was extracted and analyzed to evaluate renal and hepatic functions. Serum creatinine (Scr) levels were quantified using a Creatinine Assay Kit (C011-2-1, Nanjing Jiancheng, Nanjing, China) while alanine aminotransferase (ALT) levels were determined with an ALT Assay Kit (C009-2-1, Nanjing Jiancheng) and aspartate aminotransferase (AST) levels were assessed using an AST Assay Kit (C010-2-1, Nanjing Jiancheng), all in accordance with the manufacturer's protocols.

Oxygen and glucose deprivation/reoxygenation model and drug treatment

BV2 microglial cells were harvested in a humid environment at 37 ℃ with 5% CO_2 in DMEM (Gibco, Waltham, MA, USA) added with 10% fetal bovine serum (FBS), 100 U/mL penicillin, and 100 μg/mL streptomycin. The BV2 cells were treated with glucose-free Earle's balanced salt solution and then incubated for 4 hours at 37 ℃ in a chamber with 95% N_2 and 5% CO_2 to establish an oxygen and glucose deprivation/reoxygenation (OGD/R) model. The same washing and medium changes were applied to control cells, but they were perpetually maintained in full culture media at a temperature of 37 ℃ with 5% CO_2 and 95% air. Reperfusion was allowed in normal conditions for 12 to 24 hours (31). Cells were treated with different concentrations of RU.521 (0.5, 1 μM) or vehicle (DMSO) from 2 hours before oxygen-glucose deprivation to the time they were harvested (32).

Western blot analysis

The western blot was performed following conventional procedures. In a nutshell, the cells or the ischemic cortex were lysed with cold RIPA buffer (P0013B, P0013C, Beyotime) containing 1 mM phenylmethylsulfonyl (ST506, Beyotime). Protein concentrations were quantified using bicinchoninic acid reagent (P0010S; Beyotime); subsequently, equal amounts of protein samples were separated by 12.5% sodium dodecyl sulphate-polyacrylamide gel electrophoresis (SDS-PAGE) and transferred onto polyvinylidene fluoride (PVDF) membranes (Millipore, Billerica, MA, USA) with a pore size of 0.45 mm. After 1 hour of blocking with 5% skimmed milk at room temperature, the membranes were incubated within primary antibodies overnight at 4 ℃. Primary antibodies used for western blot were anti-cGAS antibody (1:1,000, A8335, ABclonal), anti-STING antibody (1:1,000, 19851-1-AP, Proteintech, Wuhan, China), anti-NLRP3 antibody (1:1,000, YT5382, Immunoway, Plano, TX, USA), anti-ASC antibody (1:1,000, ab175449, Abcam), anti-caspase1 antibody (1:1,000, 22915-1-AP, Proteintech), anti-gasdermin D (GSDMD) antibody (1:1,000; 39754, CST), anti-IL-18 antibody (1:2,000, 10663-1-AP, Proteintech), anti-IL-1β antibody (1:1,000, AF-501-SP, R&D, Minneapolis, MN, USA), anti-inducible nitric oxide synthase (iNOS) antibody (1:1,000, 13210, CST), anti-Arg1 antibody (1:3,000, 16001-1-AP, Proteintech) and anti-β-actin antibody (1:1,000, 22915-1-AP, Proteintech). After three rounds of washing with Tris-buffered saline containing Tween 20, the membranes were transferred to and incubated at room temperature for 2 hours with horseradish peroxidase (HRP)-anti-rabbit/mouse IgG (1:2,000, A0216/A0208, Beyotime). After enhanced chemiluminescence (ECL) (PK10001, Proteintech) development, the absorbance value of the bands was

Table 1 The primers used in qRT-PCR

Genes	Forward sequence (5'-3')	Reverse sequence (5'-3')
cGAS	GCGTCTTCTTCAGTCATACTTC	CTGGTCTACAGAGGGAGTTACA
STING	CTGGCATCAAGAATCGGGTT	GCTTTGGCATCCTGTGACAT
NLRP3	GACTGCGAGAGATTCTACAGC	CCTCCTCTTCCAGCAAATAGT
Caspase1	ACAAGGCACGGGACCTATG	TCCCAGTCAGTCCTGGAAATG
GSDMD	CTGTATGCTGAGGTGAAGGCT	GGGCTGGTCCTGTAAAATCTT
ASC	ACGGAGTGCTGGATGCTTTG	TTGTCTTGGCTGGTGGTCTCT
IL-18	CTGGAATCAGACAACTTTGG	GTCAACGAAGAGAACTTGGTC
IL-1β	TACATCAGCACCTCACAAGC	AGAAACAGTCCAGCCCATACT
β-actin	CCTCTATGCCAACACAGT	AGCCACCAATCCACACAG

qRT-PCR, quantitative real-time polymerase chain reaction; cGAS, cyclic GMP-AMP synthase; STING, stimulator of interferon genes; GSDMD, gasdermin D.

analyzed with ImageJ software.

Quantitative real-time polymerase chain reaction (qRT-PCR)

Total RNA of rat cortical tissues and cell lines was isolated using TRIzol reagent (R401-01, Vazyme, Nanjing, China). Complementary DNA (cDNA) was synthesized using HiScript III RT SuperMix for qPCR kit (R323-01, Vazyme) according to the manufacturer's instruction. The cDNA was used as the template for qRT-PCR, which was performed using ChamQ Universal SYBR qPCR Master Mix (Q711, Vazyme) on ABI 7500 Real-Time PCR System (Thermo Fisher, Waltham, MA, USA). Target gene expression was analyzed using the $2^{-\Delta\Delta Ct}$ method, with β-actin mRNA as the internal control. All the primer sequences are listed in *Table 1*.

Statistical analysis

The experimental data were presented as mean ± standard error of the mean (SEM). One-way analysis of variance (ANOVA), with Bonferroni's test was used to compare multiple independent groups. The histograms involved in this study were drawn using GraphPad Prism 8.0 software.

Results

cGAS signaling is activated in microglia after HIE modeling

To study the role of cGAS signaling in HIE, we first established an animal model using neonatal SD rats and determined the expression of cGAS in brain tissues (*Figure 1A*). When compared with the sham group, the protein expression level of cGAS were up-regulated in brain infarct side of HIE pups, with peak level observed at 6 hours after modeling, and we also noticed that cGAS seemed falling down between 24 to 48 hours (*Figure 1B*).

To figure out the cell types that express cGAS in the brain cortex, we next examined the location of cGAS. Iba1, Neun, and GFAP were used to mark microglia, neurons, and astrocytes, respectively (33-35). Double immunofluorescence staining indicated that cGAS primarily colocalized with Iba1 and sparingly with GFAP, but not with Neun. Furthermore, compared to the contralateral cortex, the microglia in the ipsilateral defined by Iba1 were amoeba-like and with a roundish body, indicating that they were M1 microglia (*Figure 2*).

RU.521 inhibits cGAS signaling, NLRP3 inflammasome, and pyroptosis after OGD/R

Since cGAS was highly expressed in microglia in the *in vivo* model, a microglia cell line BV2 was chosen to build an OGD/R model to mimic HIE injury *in vitro*. We next examined the effect of RU.521 on the transcription of cGAS signaling-related molecules, including cGAS and STING, in BV2 cells at various time points after OGD/R insult. The results of real-time PCR demonstrated that the transcriptions of cGAS and STING were significantly up-regulated 12 and 24 hours after reoxygenation, while pre-

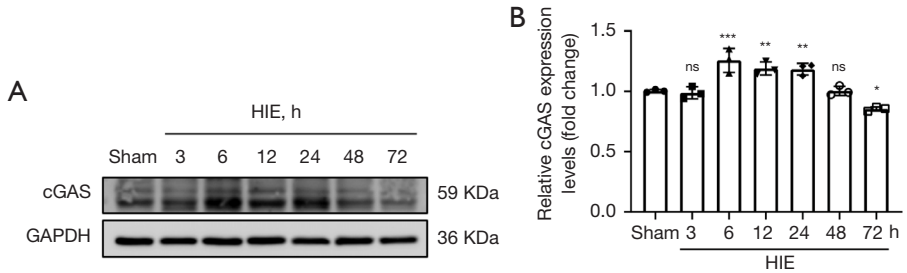

Figure 1 Time course of cGAS expression in brain tissues of neonatal rats with HIE. (A,B) Representative images and quantitative analysis of western blot analysis of cGAS in brain tissues of neonatal rats with HIE at different time points. Data are presented as mean ± SEM; n=3. *, P<0.05; **, P<0.01; ***, P<0.001. ns, no significance; cGAS, cyclic GMP-AMP synthase; HIE, hypoxic-ischemic encephalopathy; SEM, standard error of the mean.

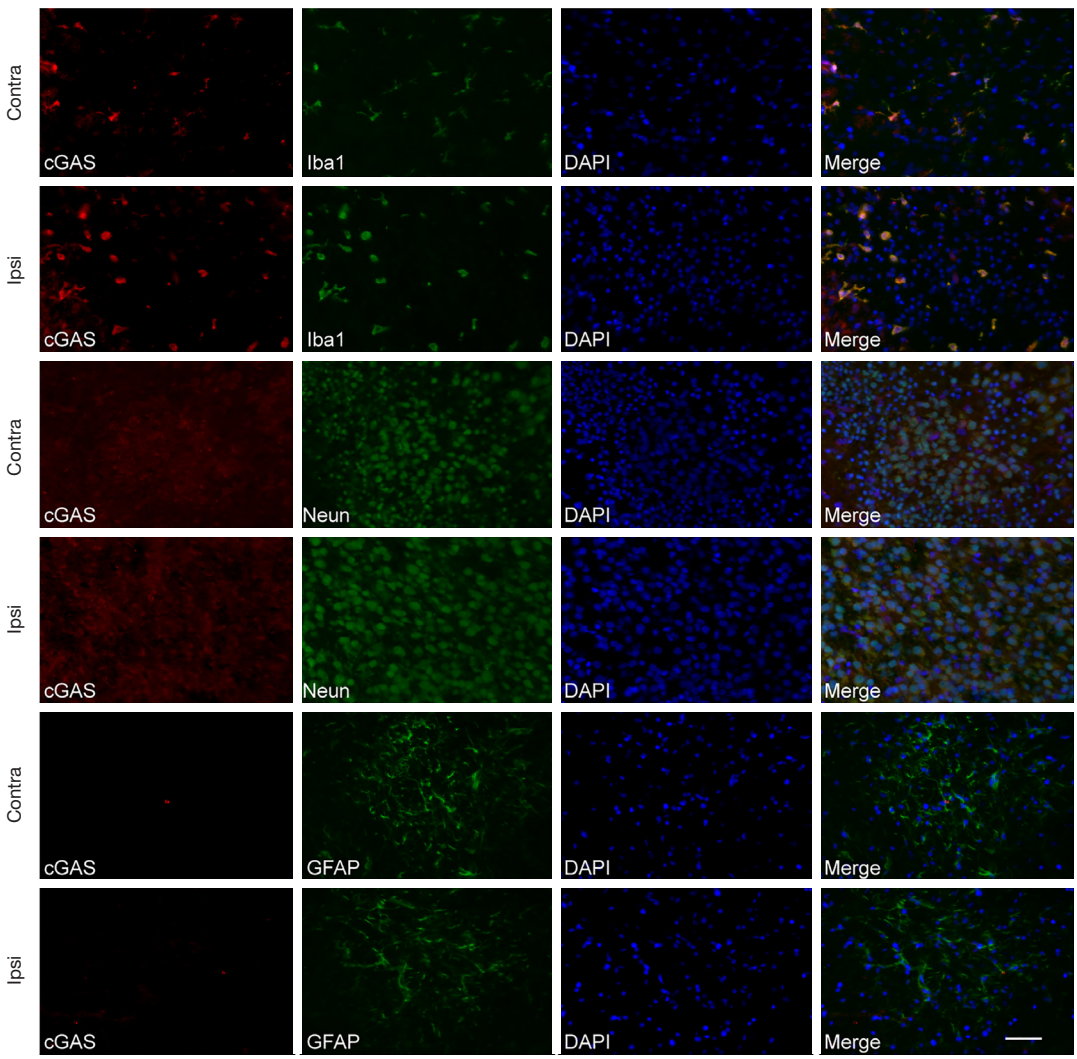

Figure 2 cGAS mainly localizes in the microglia after HIE. Double immunofluorescence staining indicated the cGAS colocalized mainly with Iba1 and to a lesser extent with Neun but not GFAP. Scale bar: 50 μm. Contra, contralateral; Ipsi, ipsilateral; cGAS, cyclic GMP-AMP synthase; HIE, hypoxic-ischemic encephalopathy; GFAP, glial fibrillary acidic protein.

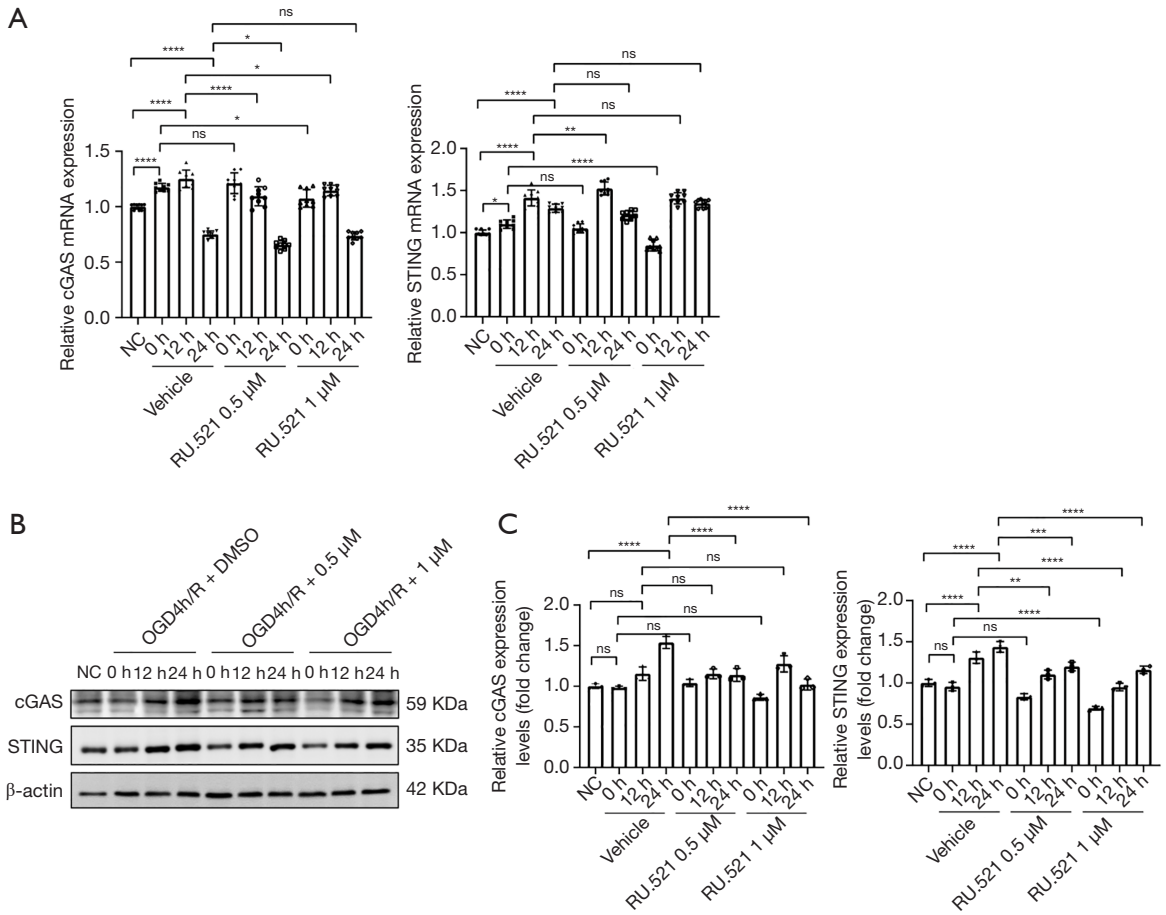

Figure 3 RU.521 inhibits cGAS/STING signaling in BV2 cells after OGD/R. (A) Real-time PCR analysis of expression of cGAS and STING in BV2 treated with RU.521 (0.5, 1 μM) for 12 or 24 h. (B,C) Representative western blot images and quantitative analysis of cGAS and STING in BV2 cells treated with RU.521 (0.5, 1 μM) for 12 or 24 h. Data are presented as mean ± SEM; n=3–9. *, P<0.05; **, P<0.01; ***, P<0.001; ****, P<0.0001. ns, no significance; cGAS, cyclic GMP-AMP synthase; NC, negative control; STING, stimulator of interferon genes; OGD/R, oxygen and glucose deprivation/reoxygenation; SEM, standard error of the mean.

treatment of RU.521 (0.5 μM) dramatically reduced the expression of both molecules (*Figure 3A*). In consistency with the changes on the transcription level, western blot analysis indicated that the protein expression of cGAS and STING was also significantly enhanced by reoxygenation and reduced by RU.521 treatment (*Figure 3B,3C*).

NLRP3 is another key player in HIE-associated inflammatory response. However, it is currently unclear whether RU.521 treatment could influence NLRP3-related pyroptosis of microglia in the OGD/R model. To clarify this issue, we first examined the effect of RU.521 on the transcription of pyroptosis-related molecules, including NLRP3, caspase1, ASC, GSDMD, IL-1β, and IL-18. The results showed that reoxygenation significantly enhanced the transcription of all these genes in BV2 cells, which were down-regulated by pre-treatment of RU.521 in BV2 cells (*Figure 4*). Meanwhile, the impact of reoxygenation and RU.521 on the protein levels of these genes in BV2 cells were measured using western blot and the results were consistent with the findings of mRNAs. More importantly, we observed that the levels of cleaved form of caspase1 (p20) and GSDMD (GSDMD-N) were also suppressed by treatment of RU.521 (*Figure 5*), indicating an inhibitory role of RU.521 for reoxygenation induced pyroptosis. Moreover, the significant down-regulation of the maturation of pro-inflammatory cytokines, IL-1β (p17) and IL-18 (p17), after treatment of RU.521 demonstrated that the drug had a suppressive role in the production of NLRP3 inflammasome

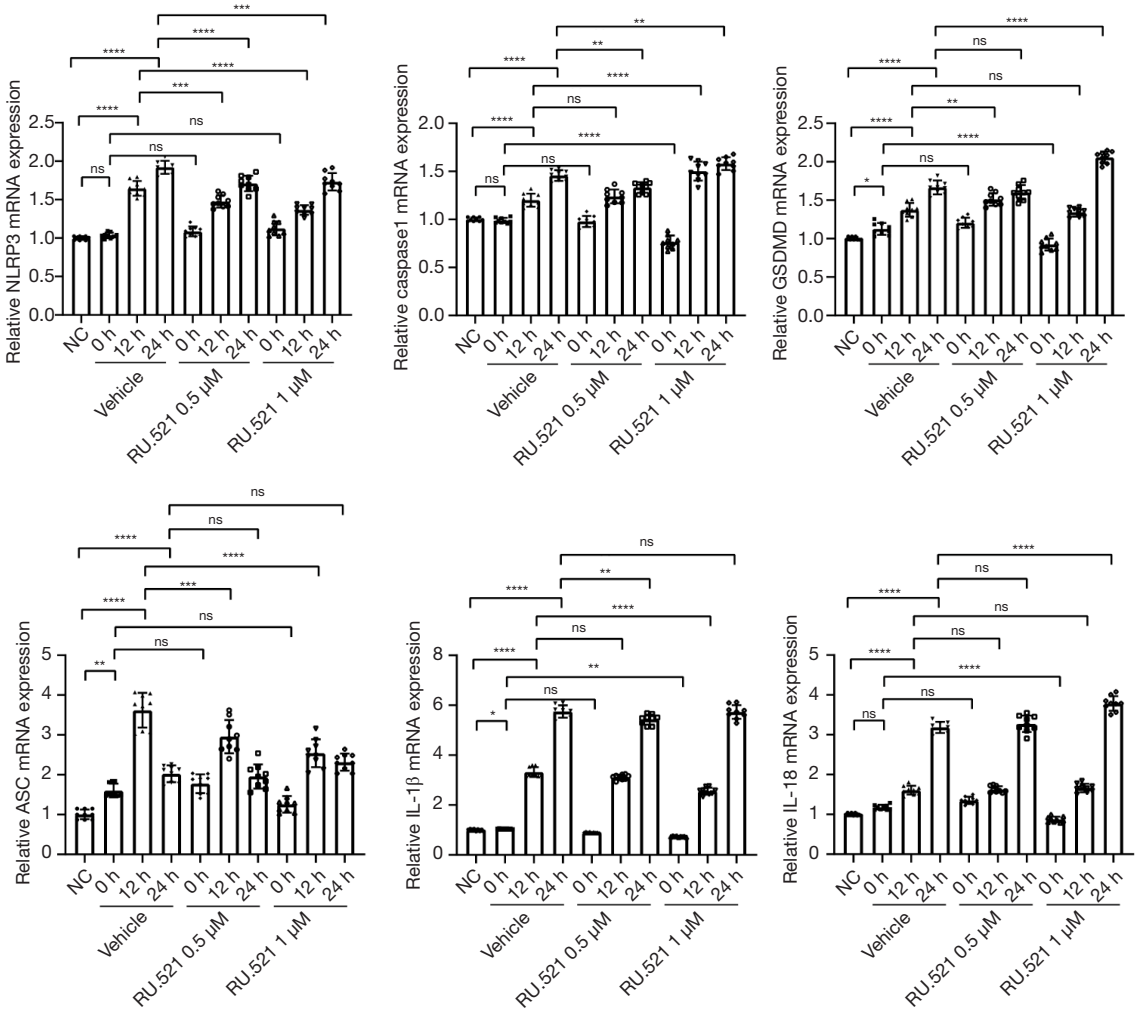

Figure 4 RU.521 inhibits mRNA expression of NLRP3 inflammasome and proinflammatory cytokines in BV2 cells after OGD/R. Real-time PCR analysis of expression of NLRP3, caspase1, ASC, GSDMD, IL-18 and IL-1β in BV2 treated with RU.521 (0.5, 1 μM) for 12 or 24 h. Data are presented as mean ± SEM; n=9. *, P<0.05; **, P<0.01; ***, P<0.001; ****, P<0.0001. ns, no significance; NC, negative control; NLRP3, NOD-like receptor protein 3; GSDMD, gasdermin D; OGD/R, oxygen and glucose deprivation/reoxygenation; PCR, polymerase chain reaction; SEM, standard error of the mean.

mediated pro-inflammatory cytokines. These results indicate that RU.521 can inhibit cGAS signaling and thus attenuate NLRP3-mediated pyroptosis and the production of pro-inflammatory cytokines *in vitro*.

We discovered that cGAS was more likely to be detected in M1 microglia in our initial *in vivo* experiment, thus we investigated the effect of RU.521 on BV2 polarization. iNOS is the marker of M1 macrophage and Arg1 (Arginase 1) is the marker of M2 macrophage. The results demonstrated that both iNOS and Arg1 increased after the OGD/R insult, and they changed in the same direction following RU.521 intervention. While there was still a discernible difference in the degree of increase, the latter increased even more especially 12 hours after reoxygenation (*Figure 6*). The results show that RU.521 can increase M2 polarization *in vitro*.

RU.521 alleviates hypoxic ischemic brain damage

The above findings prompted us to investigate the potential *in vivo* effect of RU.521. We thus established a rat model of HIE and administered RU.521 via peritoneal injection

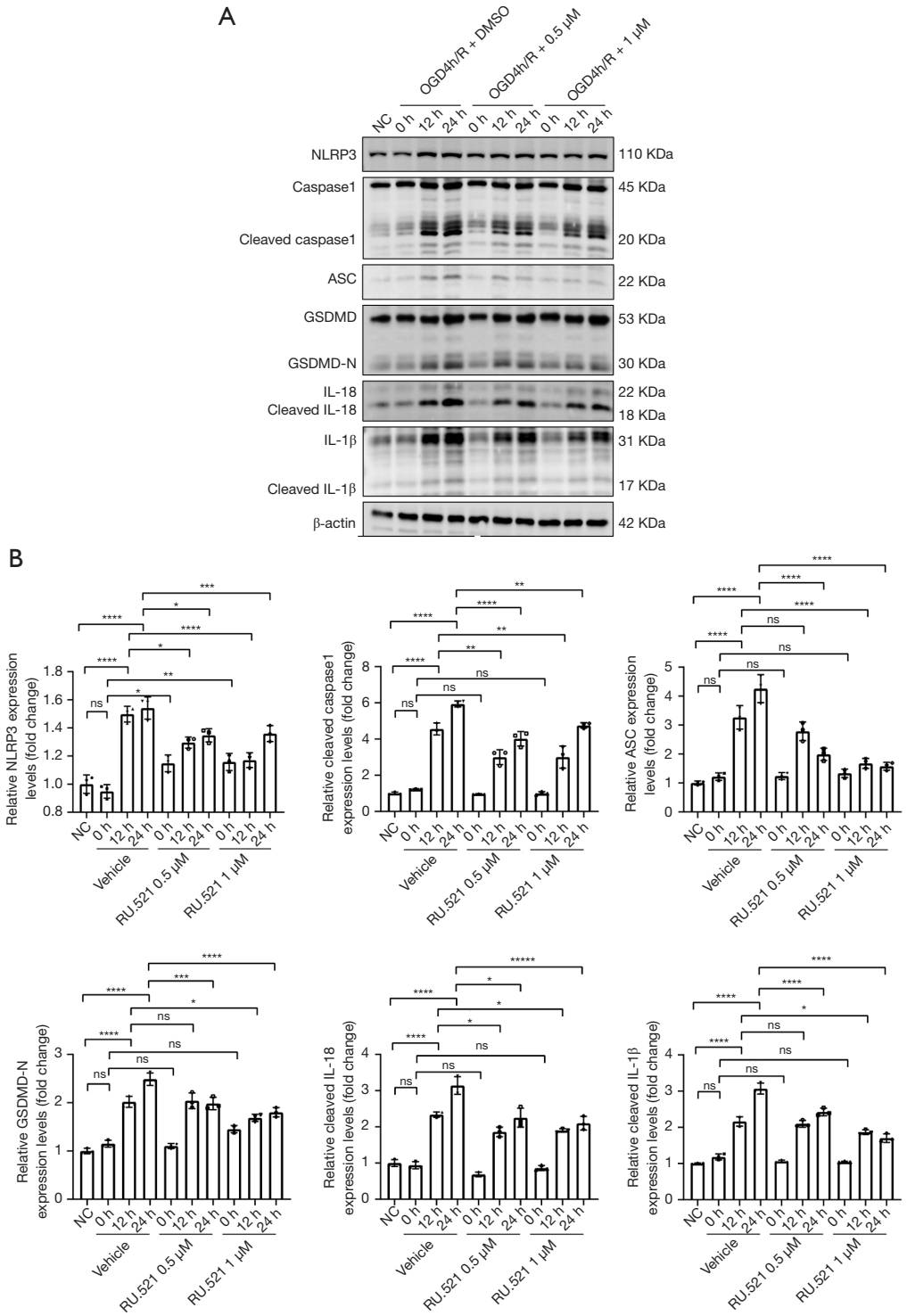

Figure 5 RU.521 inhibits NLRP3-mediated pyroptosis in BV2 cells after OGD/R. (A,B) Representative western blot images and quantitative analysis of NLRP3, cleaved caspase1, ASC, GSDMD-N, cleaved IL-18 and cleaved IL-1β in BV2 treated with RU.521 (0.5, 1 μM) for 12 or 24 h. Data are presented as mean ± SEM; n=3. *, P<0.05; **, P<0.01; ***, P<0.001; ****, P<0.0001. ns, no significance; NC, negative control; NLRP3, NOD-like receptor protein 3; GSDMD, gasdermin D; OGD/R, oxygen and glucose deprivation/reoxygenation; DMSO, dimethyl sulfoxide; SEM, standard error of the mean.

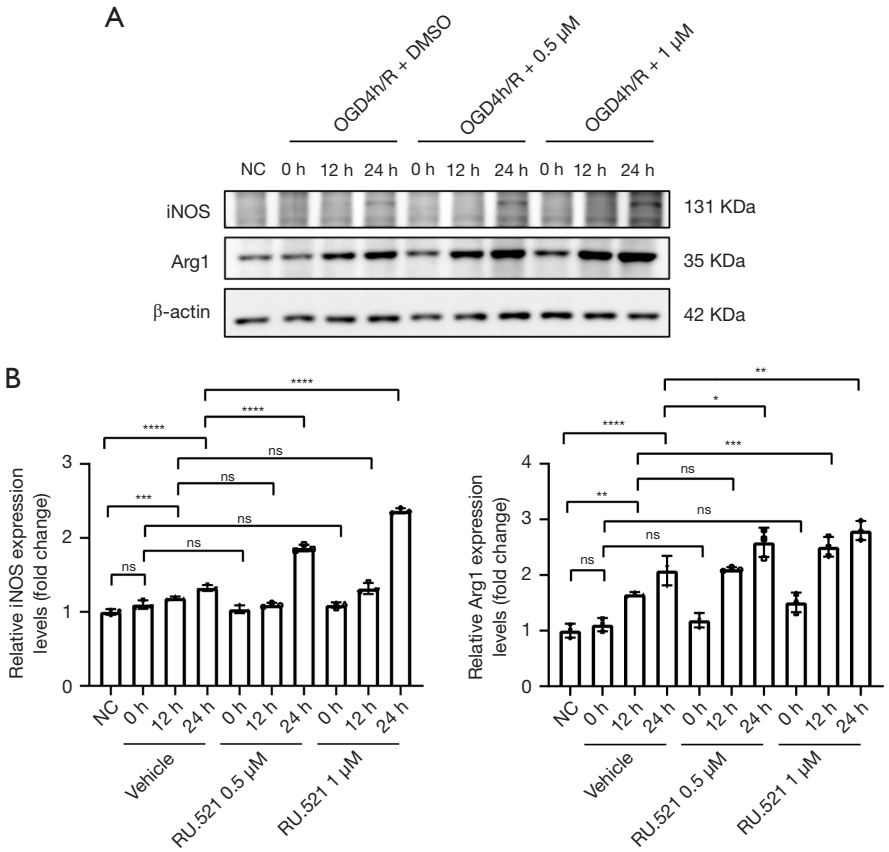

Figure 6 RU.521 promotes M2 phenotypic polarization of BV2 cells after OGD/R. (A,B) Representative western blot images and quantitative analysis of iNOS and Arg1 in BV2 cells treated with RU.521 (0.5, 1 μM) for 12 or 24 h. Data are presented as mean ± SEM; n=3. *, P<0.05; **, P<0.01; ***, P<0.001; ****, P<0.0001. ns, no significance; iNOS, inducible nitric oxide synthase; OGD/R, oxygen and glucose deprivation/reoxygenation; DMSO, dimethyl sulfoxide; NC, negative control; SEM, standard error of the mean.

as shown in the schematic (*Figure 7A*). HIE pups were administered 2.5, 5 and 10 mg/kg RU.521 intraperitoneally. TTC staining was performed to evaluate the infarct volume in the sham, HIE, and HIE + RU.521 groups. The sham group had normal brain tissue morphology. The results showed that even in the low-dose drug group, the infarction volume of the brain [22.37%, 95% confidence interval (CI): 21.01–23.73%] was significantly lower than that in the HIE group (30.03%, 95% CI: 28.09–31.97%), and the infarct size was further reduced in the medium-dose drug group (17.40%, 95% CI: 16.29–18.51%), but there was no significant difference compared with the high-dose group (17.50%, 95% CI: 16.46–18.54%) (*Figure 7B*). This analysis also revealed that 5 mg/kg of RU.521 was the most efficacious dose for reducing the volume of HIE-induced cerebral infarction in rats (*Figure 7C*). As a result, 5 mg/kg RU.521 was chosen for further tests. In addition to brain damage, hypoxia also causes liver and kidney damage. In this experiment, the Scr content and ALT and AST activities of HIE model rats were significantly higher than those of the sham operation group. After RU.521 treatment, although there was no statistical difference, these indicators still showed a downward trend (*Figure 7D*). Besides detecting blood biochemistry to assess RU.521 drug toxicity, kidney, liver, and heart tissues were collected after pups were sacrificed, and organ damage was observed by H&E staining. The results showed that there was no significant difference in the heart and liver histology of the rats in each group. However, necrosis and detachment of tubular epithelial cells occurred at the junction of the cortex and medulla of the kidneys of rats in the HIE group, and the basement membrane was exposed, while no similar situation was observed in the RU.521 intervention group (*Figure 7E*). The number of TUNEL-positive cells

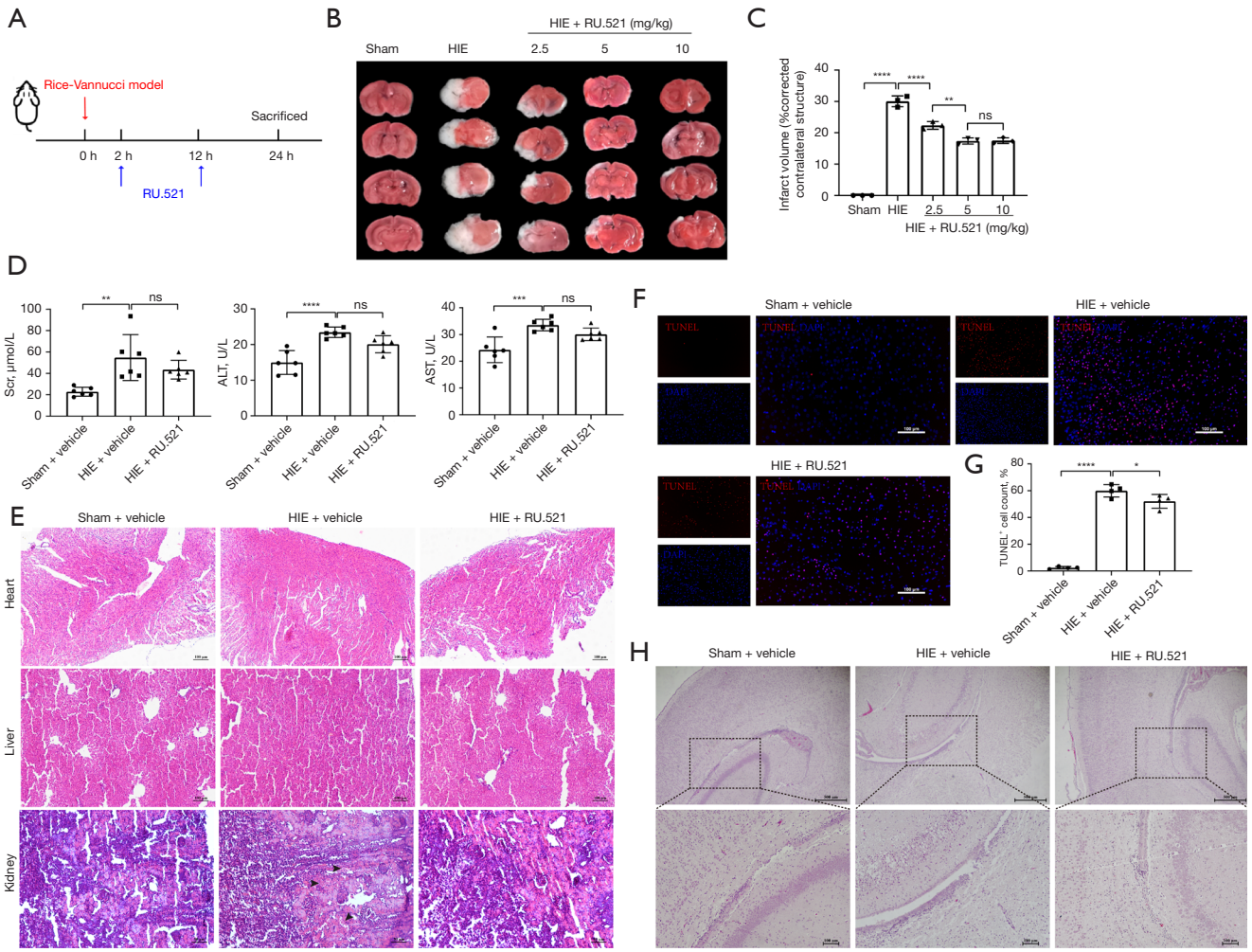

Figure 7 RU.521 reduces brain infarct volume and improves pathological damage after HIE. (A) Schedule of *in vivo* experimental procedure. (B) Representative images of TTC staining of brain tissues at different doses of RU.521. (C) Percentage analysis of infarct volume in brain tissues of each group. (D) Detection of Scr, ALT and AST in serum. (E) Representative H&E staining pictures of heart, kidney and liver sections from each group. Arrowheads indicate tubular injury. Scale bar: heart and liver, 100 μm; kidney, 50 μm. (F) Representative pictures of TUNEL staining. Scale bar: 100 μm. (G) Quantitative analysis of TUNEL-positive cells in diverse groups. (H) Representative images of H&E staining of brain tissues 24 h after HIE modeling. Scale bar: top, 500 μm; bottom, 100 μm. Data are presented as mean ± SEM; n=3–6. *, P<0.05; **, P<0.01; ***, P<0.001; ****, P<0.0001. ns, no significance; HIE, hypoxic-ischemic encephalopathy; TTC, 2,3,5-triphenyl tetrazolium chloride; H&E, hematoxylin and eosin; Scr, serum creatinine; ALT, alanine aminotransferase; AST, aspartate aminotransferase.

in the ipsilateral cerebral cortex of the rescue group was also significantly reduced (*Figure 7F,7G*). H&E staining showed that the neurons and glial cells in the Sham group had normal morphology, clear nucleoli, and no cell edema. There was no hemorrhage, necrosis, or edema in the interstitium. While in the HIE group, the cortical cells were swollen and prominent, and some nuclei were pyknotic. The interstitial tissue was loose and edematous, and the extracapillary space was widened. RU.521 treatment significantly improved this injury after HIE, and the brain tissue morphology of the rescued group was closer to that of the sham group (*Figure 7H*).

RU.521 attenuates HIE-induced neuroinflammation

We then examined the expression changes of cGAS/STING pathway molecules in HIE rats. Western blot results showed that the protein levels of cGAS and STING were significantly enhanced in brain tissues of rat pups

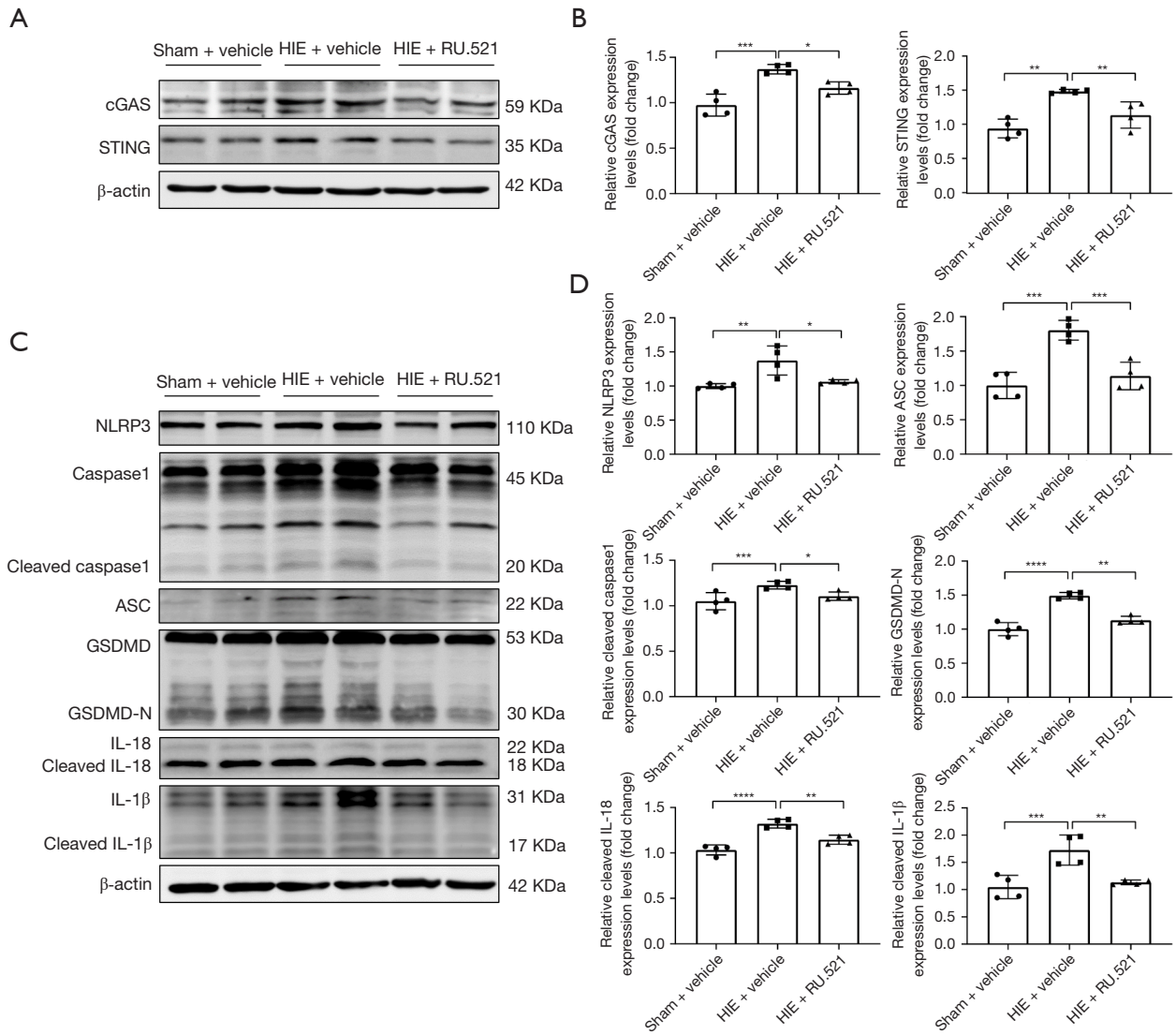

Figure 8 RU.521 inhibits HIE-induced expression of cGAS, and NLRP3 inflammasome- and pyroptosis-associated molecules. Rat pups received intraperitoneal injection of RU.521 (5 mg/kg) or an equal volume of vehicle at 2 and 12 h post-HIE. (A,B) Representative western blot images quantitative analysis of cGAS and STING. (C,D) Representative western blot images quantitative analysis of NLRP3, caspase1, cleaved caspase1, ASC, GSDMD, GSDMD-N, IL-18, cleaved IL-18, IL-1β, and cleaved IL-1β in the brain cortex of indicated groups. Data are presented as mean ± SEM; n=4. *, P<0.05; **, P<0.01; ***, P<0.001; ****, P<0.0001. cGAS, cyclic GMP-AMP synthase; STING, stimulator of interferon genes; HIE, hypoxic-ischemic encephalopathy; NLRP3, NOD-like receptor protein 3; GSDMD, gasdermin D; SEM, standard error of the mean.

on day 1 post-HIE (*Figure 8A,8B*), while intraperitoneal injection of RU.521 into rat pups significantly suppressed the expression of both molecules in the brain tissues (*Figure 8A,8B*). Similar to the results in BV2 cells, the levels of pyroptosis-related genes and NLRP3 inflammasome mediated pro-inflammatory cytokines in brain tissues of rat pups were up-regulated by ischemic hypoxia injury and were down-regulated by intraperitoneal injection of RU.521 (*Figure 8C,8D*). Here, the results demonstrated that the cGAS/STING/NLRP3 axis was highly activated after modeling and RU.521 significantly reduced cGAS/STING signaling and NLRP3 inflammasome mediated pyroptosis

in brain cerebral cortex of HIE rats.

Discussion

In this study, we found that the cGAS/STING axis was significantly elevated in an HIE rat model, which correlated with increased neuroinflammation in the brain. Blocking cGAS with a specific inhibitor, RU.521, significantly reduced inflammatory conditions in the brain by inhibiting the level of STING, the activation of NLRP3 inflammasome and GSDMD mediated microglial pyroptosis. Besides, RU.521 promoted the switching of BV2 cells towards the M2 phenotype. Our findings revealed a link between the cGAS/STING pathway and the NLRP3/GSDMD/pyroptosis pathway in neonatal HIE.

Our study found that in the HIE model of 7-day-old SD rats, cGAS protein expression increased significantly after 6 hours and began to decrease at 24 to 48 hours. A previous study has shown that the most serious brain injury is induced 24 hours after HIE insult (36). Therefore, in this part of the animal experimental study, we selected this time point to detect the changes of cGAS/STING/NLRP3 protein levels in the cerebral cortex of rats after the establishment of HIE model. The results of this study showed that cGAS/STING, NLRP3 related pyroptosis genes including ASC, caspase1, GSDMD, IL-18, and IL-1β were up-regulated after modeling. Blocking cGAS with RU.521 not only down-regulated the downstream STING expression, but also significantly reduced the generation of NLRP3 inflammasome and microglial pyroptosis. Both cGAS/STING and NLRP3 inflammasome have been shown to regulate inflammatory responses in many diseases. This study did not interfere with NLRP3 to observe the changes of cGAS/STING pathway. However, it has been shown that the expression levels of IL-1β and IL-18, the downstream inflammatory cytokines of NLRP3 inflammasome, were significantly decreased in human pulmonary microvascular endothelial cells (HPMVECs) treated with MCC950, while the expression levels of cGAS and STING were not remarkably decreased (37). Combining the results of the two experiments, we hypothesize that the cGAS/STING pathway may act as an upstream regulator of NLRP3 inflammasome, which in turn regulates inflammatory responses in HIE. Activation of the NF-κB signaling pathway is a key regulatory mechanism mediating the NLRP3 inflammasome initiation process, and the NF-κB signaling pathway is also one of the downstream inflammatory signaling pathways after STING activation (38,39). Therefore, NF-κB-mediated transcriptional activation of NLRP3 inflammasome-related proteins may be an important bridge between the cGAS-STING axis and NLRP3 inflammasome-mediated microglial pyroptosis. In addition, studies have found that STING can bind to NLRP3 in the endoplasmic reticulum and improve NLRP3 localization to promote the formation of NLRP3 inflammasomes (40,41). Moreover, STING can interact with NLRP3 and weaken the K48 and K63-linked polyubiquitination of NLRP3 to induce the activation of NLRP3 inflammasomes (41). While the specific interacting mechanisms between the two immune response-related pathways, the specific functions, and potential new regulatory mechanisms of these two pathways in HIE still need further research.

As key innate immune system receptors, Toll-like receptors (TLRs) and cGAS-STING both play a role in the occurrence and development of neuroinflammation (42,43). Numerous studies have shown that TLR4/MyD88/NF-κB signaling pathway plays a crucial role in HIE disease, and some natural compounds can protect HIE by inhibiting different nodes of this pathway (44-46). In a human immunodeficiency virus (HIV)-related study, researchers have found that the TLR with cGAS crosstalk between signaling pathways, showing that cGAS-dependent IFN-1 production requires the participation of a second signal generated after TLR pathway activation, namely the fusion of two different types of innate immune signaling pathways can amplify the signal output (47). In addition, a study has shown that TLR4/cGAS/STING axis also exists in hepatocellular carcinoma *in vitro* model (48). However, no studies have shown the crosstalk between TLRs and cGAS/STING pathways in HIE disease, and more in-depth studies are needed to delineate the signal transduction network.

Highly production of pro-inflammatory cytokines often leads to poor clinical prognosis (49). However, excessive neutralization or blockade of cytokines actually increases adverse consequences and faces challenges in the actual clinical translation process (50). For example, canakinumab (an anti-IL-1β antibody) has already been approved for treating autoimmune diseases. While due to the pleiotropic effects of IL-1β on immunomodulatory processes, blindly inhibiting its activity often leads to serious side effects such as infection, allergy, and immunosuppression in actual clinical application (51). Based on the fact that cGAS senses specific double-stranded DNA and then causes

related inflammatory responses, we believe that using the specific inhibitor RU.521 by targeting cGAS to regulate the inflammatory cascade and improve inflammatory injury after HIE may have greater safety. Yet this speculation needs to be further validated in further animal-based studies and preclinical studies.

With the progress of hypoxic-ischemic brain injury, microglia will dynamically change its phenotype and function, and gradually change to the pro-inflammatory M1 phenotype. The increased polarization of pro-inflammatory microglia can aggravate brain injury, hinder neuronal regeneration, and interfere with the repair of neurological function after injury. Our study shows that when HIE occurs, microglia are activated in the cerebral cortex on the infarcted side, mostly showing a pro-inflammatory M1 phenotype. Although we did not examine the effect of RU.521 on microglial polarization *in vivo*, RU.521 treatment was significantly involved in the regulation of microglial polarization in the *in vitro* model of OGD/R, and Arg1 expression was more significant than iNOS, suggesting that the resting microglial cells tend to transition to the anti-inflammatory M2 phenotype. Further research is required to understand the detailed mechanisms.

The present study, however, has certain limitations that necessitate further investigation. Our study found that cGAS was highly expressed in rat HIE and the use of the small molecule inhibitor RU.521 could inhibit the activation of downstream pathways. However, there has been no study on the expression pattern of cGAS in clinical human HIE, which is also the focus of our further study. Cerebrospinal fluid (CSF) is the most valuable extracellular fluid in the study of the central nervous system. In addition to sugars, proteins, electrolytes and other components, CSF also contains extracellular vesicles (EVs), which carry bioactive substances such as lipids, nucleic acids and proteins (52). CSF EVs may play a role in communication of central nervous system. Although we have not been able to study the expression of cGAS in EVs, it is gratifying that double-strand DNA (dsDNA) of the cGAS/STING pathway and activated STING protein can be transported to bystander cells through EVs (53,54). Despite the limited research, EVs in CSF still provide us with inspiration to detect whether there is activation of the cGAS/STING/NLRP3 pathway in human HIE diseases. The purpose of this study is to determine the cGAS for future medication development goals. Although RU.521 was found to be a good inhibitor of the cGAS/STING pathway in our study and some other rodent studies, it is a poor human cGAS inhibitor (55). Subsequent studies will evaluate different cGAS inhibitors in animal models with particular emphasis on VENT-03, a first-in-class cGAS inhibitor—to see if it has a therapeutic effect on HIE (56).

Conclusions

This study demonstrates that the cGAS/STING pathway is up-regulated in both animal and cellular models of HIE and plays a role in neuroinflammation, possibly through activation of the NLRP3 inflammasome and associated microglial pyroptosis, as well as regulation of M1/M2 polarization in microglia. Our results also show that the changes induced by HIE insult can be alleviated by treatment with RU.521, which provides that cGAS is a promising therapeutic target for the treatment of neuroinflammation in HIE.

Acknowledgments

Funding: This work was supported partially by Nantong Science and Technology Project (Nos. MS12020004, MS2023019) and the Nantong Municipal Commission of Health and Family Planning (No. MS2022029).

Footnote

Reporting Checklist: The authors have completed the ARRIVE reporting checklist. Available at https://tp.amegroups.com/article/view/10.21037/tp-24-148/rc

Data Sharing Statement: Available at https://tp.amegroups.com/article/view/10.21037/tp-24-148/dss

Peer Review File: Available at https://tp.amegroups.com/article/view/10.21037/tp-24-148/prf

Conflicts of Interest: All authors have completed the ICMJE uniform disclosure form (available at https://tp.amegroups.com/article/view/10.21037/tp-24-148/coif). The authors have no conflicts of interest to declare.

Ethical Statement: The authors are accountable for all aspects of the work in ensuring that questions related to the accuracy or integrity of any part of the work are appropriately investigated and resolved. All animal experiments were carried out under the approval of the Animal Ethics Committee of Nantong University, China

(approval No. S20230610-099) and applied with the guide of the Animal Care and Use Committee of Nantong University.

References

1. Juul SE, Voldal E, Comstock BA, et al. Association of High-Dose Erythropoietin With Circulating Biomarkers and Neurodevelopmental Outcomes Among Neonates With Hypoxic Ischemic Encephalopathy: A Secondary Analysis of the HEAL Randomized Clinical Trial. JAMA Netw Open 2023;6:e2322131.
2. Zheng Y, Li L, Chen B, et al. Chlorogenic acid exerts neuroprotective effect against hypoxia-ischemia brain injury in neonatal rats by activating Sirt1 to regulate the Nrf2-NF-κB signaling pathway. Cell Commun Signal 2022;20:84.
3. Ramirez A, Peyvandi S, Cox S, et al. Neonatal brain injury influences structural connectivity and childhood functional outcomes. PLoS One 2022;17:e0262310.
4. He X, Zhang T, Zeng Y, et al. Sodium butyrate mediates histone crotonylation and alleviated neonatal rats hypoxic-ischemic brain injury through gut-brain axis. Front Microbiol 2022;13:993146.
5. Walas W, Wilińska M, Bekiesińska-Figatowska M, et al. Methods for assessing the severity of perinatal asphyxia and early prognostic tools in neonates with hypoxic-ischemic encephalopathy treated with therapeutic hypothermia. Adv Clin Exp Med 2020;29:1011-6.
6. Park YJ, Borlongan CV, Dezawa M. Cell-based treatment for perinatal hypoxic-ischemic encephalopathy. Brain Circ 2021;7:13-7.
7. Liu SJ, Liu XY, Li JH, et al. Gastrodin attenuates microglia activation through renin-angiotensin system and Sirtuin3 pathway. Neurochem Int 2018;120:49-63.
8. Guo J, Zhang XL, Bao ZR, et al. Gastrodin Regulates the Notch Signaling Pathway and Sirt3 in Activated Microglia in Cerebral Hypoxic-Ischemia Neonatal Rats and in Activated BV-2 Microglia. Neuromolecular Med 2021;23:348-62.
9. Li X, Zhang Y, Chang J, et al. Mfsd2a attenuated hypoxic-ischemic brain damage via protection of the blood-brain barrier in mfat-1 transgenic mice. Cell Mol Life Sci 2023;80:71.
10. Fang M, Liu J, Zhang Z, et al. Chloroquine Protects Hypoxia/Ischemia-Induced Neonatal Brain Injury in Rats by Mitigating Blood-Brain Barrier Disruption. ACS Chem Neurosci 2023;14:1764-73.
11. Cohen D, Melamed S, Millman A, et al. Cyclic GMP-AMP signalling protects bacteria against viral infection. Nature 2019;574:691-5.
12. Singh RS, Vidhyasagar V, Yang S, et al. DDX41 is required for cGAS-STING activation against DNA virus infection. Cell Rep 2022;39:110856.
13. Gulla A, Morelli E, Samur MK, et al. Bortezomib induces anti-multiple myeloma immune response mediated by cGAS/STING pathway activation. Blood Cancer Discov 2021;2:468-83.
14. Wan D, Jiang W, Hao J. Research Advances in How the cGAS-STING Pathway Controls the Cellular Inflammatory Response. Front Immunol 2020;11:615.
15. Messaoud-Nacer Y, Culerier E, Rose S, et al. STING agonist diABZI induces PANoptosis and DNA mediated acute respiratory distress syndrome (ARDS). Cell Death Dis 2022;13:269.
16. Wang C, Yang T, Xiao J, et al. NLRP3 inflammasome activation triggers gasdermin D-independent inflammation. Sci Immunol 2021;6:eabj3859.
17. Toldo S, Abbate A. The NLRP3 inflammasome in acute myocardial infarction. Nat Rev Cardiol 2018;15:203-14.
18. Lin Q, Li S, Jiang N, et al. Inhibiting NLRP3 inflammasome attenuates apoptosis in contrast-induced acute kidney injury through the upregulation of HIF1A and BNIP3-mediated mitophagy. Autophagy 2021;17:2975-90.
19. Xiao Y, Zhao C, Tai Y, et al. STING mediates hepatocyte pyroptosis in liver fibrosis by Epigenetically activating the NLRP3 inflammasome. Redox Biol 2023;62:102691.
20. Zhong WJ, Liu T, Yang HH, et al. TREM-1 governs NLRP3 inflammasome activation of macrophages by firing up glycolysis in acute lung injury. Int J Biol Sci 2023;19:242-57.
21. Gamdzyk M, Doycheva DM, Araujo C, et al. cGAS/STING Pathway Activation Contributes to Delayed Neurodegeneration in Neonatal Hypoxia-Ischemia Rat Model: Possible Involvement of LINE-1. Mol Neurobiol

2020;57:2600-19.
22. Yang XL, Wang X, Shao L, et al. TRPV1 mediates astrocyte activation and interleukin-1β release induced by hypoxic ischemia (HI). J Neuroinflammation 2019;16:114.
23. Serdar M, Kempe K, Rizazad M, et al. Early Pro-inflammatory Microglia Activation After Inflammation-Sensitized Hypoxic-Ischemic Brain Injury in Neonatal Rats. Front Cell Neurosci 2019;13:237.
24. Yang L, Yu X, Zhang Y, et al. Caffeine treatment started before injury reduces hypoxic-ischemic white-matter damage in neonatal rats by regulating phenotypic microglia polarization. Pediatr Res 2022;92:1543-54.
25. Shao J, Meng Y, Yuan K, et al. RU.521 mitigates subarachnoid hemorrhage-induced brain injury via regulating microglial polarization and neuroinflammation mediated by the cGAS/STING/NF-κB pathway. Cell Commun Signal 2023;21:264.
26. Rice JE 3rd, Vannucci RC, Brierley JB. The influence of immaturity on hypoxic-ischemic brain damage in the rat. Ann Neurol 1981;9:131-41.
27. Chen X, Chen A, Wei J, et al. Dexmedetomidine alleviates cognitive impairment by promoting hippocampal neurogenesis via BDNF/TrkB/CREB signaling pathway in hypoxic-ischemic neonatal rats. CNS Neurosci Ther 2024;30:e14486.
28. Ding R, Li H, Liu Y, et al. Activating cGAS-STING axis contributes to neuroinflammation in CVST mouse model and induces inflammasome activation and microglia pyroptosis. J Neuroinflammation 2022;19:137.
29. Directive 2010/63/EU of the European Parliament and of the Council of 22 September 2010 on the protection of animals used for scientific purposes Text with EEA relevance. Official Journal of the European Union 2010;53:33-79.
30. Jin W, Zhao J, Yang E, et al. Neuronal STAT3/HIF-1α/PTRF axis-mediated bioenergetic disturbance exacerbates cerebral ischemia-reperfusion injury via PLA2G4A. Theranostics 2022;12:3196-216.
31. Zhou K, Wu J, Chen J, et al. Schaftoside ameliorates oxygen glucose deprivation-induced inflammation associated with the TLR4/Myd88/Drp1-related mitochondrial fission in BV2 microglia cells. J Pharmacol Sci 2019;139:15-22.
32. Posch W, Bermejo-Jambrina M, Steger M, et al. Complement Potentiates Immune Sensing of HIV-1 and Early Type I Interferon Responses. mBio 2021;12:e0240821.
33. Kanazawa H, Ohsawa K, Sasaki Y, et al. Macrophage/microglia-specific protein Iba1 enhances membrane ruffling and Rac activation via phospholipase C-gamma -dependent pathway. J Biol Chem 2002;277:20026-32.
34. Eng LF, Ghirnikar RS, Lee YL. Glial fibrillary acidic protein: GFAP-thirty-one years (1969-2000). Neurochem Res 2000;25:1439-51.
35. Mullen RJ, Buck CR, Smith AM. NeuN, a neuronal specific nuclear protein in vertebrates. Development 1992;116:201-11.
36. Nedelcu J, Klein MA, Aguzzi A, et al. Biphasic edema after hypoxic-ischemic brain injury in neonatal rats reflects early neuronal and late glial damage. Pediatr Res 1999;46:297-304.
37. Jiang S, Wang M, Zhao H, et al. cGAS/STING regulates inflammation of human pulmonary microvascular endothelial cells via NLRP3 inflammasome. Chinese Journal of Critical Care & Intensive Care Medicine (Electronic Edition) 2021;7:233-40.
38. Dapueto R, Rodriguez-Duarte J, Galliussi G, et al. A novel nitroalkene vitamin E analogue inhibits the NLRP3 inflammasome and protects against inflammation and glucose intolerance triggered by obesity. Redox Biol 2021;39:101833.
39. Yum S, Li M, Fang Y, et al. TBK1 recruitment to STING activates both IRF3 and NF-κB that mediate immune defense against tumors and viral infections. Proc Natl Acad Sci U S A 2021;118:e2100225118.
40. Wang Z, Hu X, Cui P, et al. Progress in understanding the role of cGAS-STING pathway associated with programmed cell death in intervertebral disc degeneration. Cell Death Discov 2023;9:377.
41. Wang W, Hu D, Wu C, et al. STING promotes NLRP3 localization in ER and facilitates NLRP3 deubiquitination to activate the inflammasome upon HSV-1 infection. PLoS Pathog 2020;16:e1008335.
42. Squillace S, Salvemini D. Toll-like receptor-mediated neuroinflammation: relevance for cognitive dysfunctions. Trends Pharmacol Sci 2022;43:726-39.
43. Paul BD, Snyder SH, Bohr VA. Signaling by cGAS-STING in Neurodegeneration, Neuroinflammation, and Aging. Trends Neurosci 2021;44:83-96.
44. Tang Z, Cheng S, Sun Y, et al. Early TLR4 inhibition reduces hippocampal injury at puberty in a rat model of neonatal hypoxic-ischemic brain damage via regulation of neuroimmunity and synaptic plasticity. Exp Neurol 2019;321:113039.
45. Le K, Wu S, Chibaatar E, et al. Alarmin HMGB1 Plays a Detrimental Role in Hippocampal Dysfunction Caused by

Hypoxia-Ischemia Insult in Neonatal Mice: Evidence from the Application of the HMGB1 Inhibitor Glycyrrhizin. ACS Chem Neurosci 2020;11:979-93.
46. Le K, Song Z, Deng J, et al. Quercetin alleviates neonatal hypoxic-ischemic brain injury by inhibiting microglia-derived oxidative stress and TLR4-mediated inflammation. Inflamm Res 2020;69:1201-13.
47. Siddiqui MA, Yamashita M. Toll-Like Receptor (TLR) Signaling Enables Cyclic GMP-AMP Synthase (cGAS) Sensing of HIV-1 Infection in Macrophages. mBio 2021;12:e0281721.
48. Sun B, Zhang Q, Sun T, et al. Radiofrequency hyperthermia enhances the effect of OK-432 for Hepatocellular carcinoma by activating of TLR4-cGAS-STING pathway. Int Immunopharmacol 2024;130:111769.
49. Martins AC, Lima IS, Pêgo AC, et al. Pro-Inflammatory Priming of the Brain: The Underlying Cause of Parkinson's Disease. Int J Mol Sci 2023;24:7949.
50. Lambertsen KL, Finsen B, Clausen BH. Post-stroke inflammation-target or tool for therapy? Acta Neuropathol 2019;137:693-714.
51. Ridker PM, Thuren T, Zalewski A, et al. Interleukin-1β inhibition and the prevention of recurrent cardiovascular events: rationale and design of the Canakinumab Anti-inflammatory Thrombosis Outcomes Study (CANTOS). Am Heart J 2011;162:597-605.
52. Sandau US, Magaña SM, Costa J, et al. Recommendations for reproducibility of cerebrospinal fluid extracellular vesicle studies. J Extracell Vesicles 2024;13:e12397.
53. Liang J, Yin H. STAM transports STING oligomers into extracellular vesicles, down-regulating the innate immune response. J Extracell Vesicles 2023;12:e12316.
54. Tkach M, Théry C. Communication by Extracellular Vesicles: Where We Are and Where We Need to Go. Cell 2016;164:1226-32.
55. Lama L, Adura C, Xie W, et al. Development of human cGAS-specific small-molecule inhibitors for repression of dsDNA-triggered interferon expression. Nat Commun 2019;10:2261.
56. Mullard A. Biotechs step on cGAS for autoimmune diseases. Nat Rev Drug Discov 2023;22:939-41.

Cite this article as: Shen H, Lu H, Mao L, Song L. Inhibition of cGAS attenuates neonatal hypoxic-ischemic encephalopathy via regulating microglia polarization and pyroptosis. Transl Pediatr 2024;13(8):1378-1394. doi: 10.21037/tp-24-148